Testing Simple Models of ENSO

CARLOS R. MECHOSO, J. DAVID NEELIN, AND JIN-YI YU

Department of Atmospheric Sciences, University of California, Los Angeles, Los Angeles, California

(Manuscript received 6 September 2001, in final form 24 July 2002)

ABSTRACT

The realistic simulation of El Niño–Southern Oscillation (ENSO) by the University of California, Los Angeles (UCLA), coupled atmosphere–ocean general circulation model (CGCM) is used to test two simple theoretical models of the phenomenon: the recharge oscillator model of Jin and the delayed oscillator model of Schopf, Suarez, Battisti, and Hirst (SSBH). The target for the simple models is provided by the CGCM results prefiltered with singular spectrum analysis to extract the leading oscillatory mode. In its simplest form, the Jin model can be reduced to two first ordinary differential equations. If the parameters of the model are fit in this reduced form, it appears to capture the period of the CGCM oscillatory mode. If the Jin model is instead fit using the individual physical balances that are used to derive it, substantial misfits to the CGCM are encountered. The SSBH model can likewise be expressed either in a condensed form or a larger set of individual physical balances with highly analogous results.

It is shown that the misfits in both simple models can be greatly reduced by introducing a spinup timescale for wind stress relative to eastern equatorial Pacific SST. In the CGCM, this spinup time appears to be associated with a combination of atmospheric and ocean mixed layer processes in a way consistent with the ''mixed mode'' regime discussed by Syu and Neelin, which is not included in the Jin and SSBH models. These appear indistinguishable in this analysis, although the latter is more sensitive to fitting.

This paper provides a bridge between work on ENSO by theoreticians and numerical modelers. The CGCM results validate the conceptual framework of the simple models by demonstrating that they can provide a plausible representation of ENSO with realistic sets of parameters. The results also suggest that, in terms of realistic ENSO variability, the framework of the simple models can be made substantially more complete by including the adjustment time between wind stress and eastern Pacific SST required by the coupled spinup of the atmosphere and the ocean mixed layer processes outside this region.

1. Introduction

A considerable number of theoretical and modeling studies have undertaken to understand the dynamics of the ENSO cycle [for review of modeling and theory, respectively, see Delecluse et al. (1998) and Neelin et al. (1998)]. Much of the theoretical work focuses on the oscillatory aspect of the phenomenon associated with the dominant spectral peak, which in observations corresponds to a period of 3 to 5 yr (Rasmusson et al. 1990; Jiang et al. 1995; Torrence and Compo 1998). The mature El Niño or La Niña are viewed as the positive and negative peak phases of the oscillation, associated with extrema of SST anomalies. The feedbacks among SST, wind, ocean current, and subsurface temperature anomalies during these phases are referred to as the Bjerknes hypothesis (Bjerknes 1966, 1969).

The reigning paradigm for the transition phases of the oscillation is that subsurface ocean temperature anomalies carry the memory of the phenomenon when little anomaly is visible at the surface. For example, the delayed oscillator model (Schopf and Suarez 1988; Suarez and Schopf 1988; Battisti and Hirst 1989; cumulatively, hereafter, SSBH) suggests that the delayed negative feedback associated with free oceanic equatorial wave propagation and reflection at the western boundary is responsible for the phase reversal of the ENSO cycle.

There has been a recent revival of the terminology of a recharge oscillator (Wyrtki 1975; Cane et al. 1986; Zebiak 1989; Jin 1997a, hereafter JIN97; An and Kang 2000). Although this is conceptually similar to the delayed oscillator theory in reference to the importance of subsurface ocean adjustment processes, the recharge oscillator theory emphasizes the importance for the phase reversal of the ENSO cycle of the buildup (i.e., charge) and release (i.e., discharge) of ocean heat content in the equatorial band. The charge and discharge are generated by the nonequilibrium between the zonal-mean ocean heat content and wind stress at the equator. The role of ocean wave propagation and reflection is left implicit in this variant of the subsurface memory paradigm. In JIN97 the terminology is essentially a misnomer, since the equation representing heat content

Corresponding author address: C. R. Mechoso, Dept. of Atmospheric Sciences, University of California, Los Angeles, Los Angeles, CA 90095-1565.
E-mail: mechoso@atmos.ucla.edu

change is a simplification of wave dynamical processes (Jin 1997b), and the process is linear, as opposed to the sudden capacitor discharge–like process alluded to in the recharge oscillator terminology. The JIN97 model differs from the SSBH delayed oscillator model in two main respects: (i) the system is simplified to two ordinary differential equations, and (ii) the oscillation depends crucially on the timescale of equilibration in the SST equation in addition to the timescale of heat content buildup. It thus gives the simplest representation of the physics of the mixed SST/ocean-dynamics mode.

Two questions come immediately to mind. First, granting that simple models include major dynamical aspects of the ENSO cycle, one can wonder about the completeness of the picture they provide. For example, consensus has not been reached on the processes responsible for carrying the memory of the oscillation during the transition phases. The slow SST model theory (Neelin 1991; Neelin and Jin 1993) contends that processes in the oceanic surface layer *not included* in the SSBH model can contribute to the memory for the phase transition, and can even provide it in some modes if subsurface processes do not. Jin and Neelin (1993) argue that the most relevant regime contains aspects of both theories: the spatial pattern of the ENSO mode is largely set by interactions captured by the slow SST mode, subsurface dynamics contributes most of the memory, while surface layer memory processes can affect the oscillation in a secondary manner. They used the somewhat cumbersome term ''mixed SST/ocean-dynamics mode'' to describe this, since it inherits characteristics from both aspects of the system. The simplifications in the JIN97 model *neglect* a feature of mixed mode dynamics, namely, that ocean–mixed layer processes away from the equatorial eastern Pacific main region can affect the oscillation. Second, one can wonder whether insight can be gained into the relative validity of two models that purport to describe the same phenomenon starting from arguably different frameworks. The plausibility of simple models is generally assessed by their success in producing oscillations with ENSO-like periods, albeit the numerical value of the period may depend on parameters that differ from those in observations from the corresponding mechanisms (Latif et al. 2001). Are the parameters chosen for the JIN97 model more realistic than those for the SSBH model?

The answers to these questions will be definitively given by contrasting model predictions with reality. Comprehensive, basinwide observational data for surface and subsurface ocean states, however, are either not yet available or very difficult to obtain. On the other hand, coupled atmosphere–ocean general circulation models (CGCMs) have demonstrated ability to capture an interannual variability that strongly resembles ENSO without appealing to artificial devices such as flux correction at the atmosphere–ocean interface. This success strongly suggests that CGCMs fields can be used for analyses of the mechanisms at work for ENSO's origin and evolution.

The University of California, Los Angeles (UCLA) CGCM is one of the models able to produce ENSO-like climate variability with reasonable frequency and amplitude (Latif et al. 2001). Yu and Mechoso (2001, hereafter YM01) analyzed a recent integration by this model. This included application of a multichannel singular spectrum analysis (M-SSA) to the evolving atmospheric and oceanic anomalies. The leading oscillatory mode—CGCM ENSO cycle—was found to be characterized by predominantly standing oscillations of SST anomalies in the eastern Pacific, almost simultaneous zonal wind stress anomalies to the west of the SST anomalies, and preceding thermocline anomalies in the west of the basin. An ocean temperature budget analysis was also performed to determine the relative importance of various ocean processes in producing subsurface ocean memory for the ENSO cycle.

The current paper uses the results of this realistic CGCM simulation to address the two questions raised above; namely, 1) How complete is the picture of ENSO provided by the SSBH and JIN97 models, and 2) how different are the models in the realistic range of parameters? Our methodology is based on fitting CGCM results to the simple model equations in order to estimate the parameters used in the latter. If a simple model provides a good fit to the CGCM this would help to validate its framework; to the extent that it does not, the methodology can help point to areas where the framework is incomplete.

We start with a brief description of the UCLA CGCM in section 2 and the simulated ENSO cycle analyzed by YM01 in section 3. Next we describe the recharge oscillator model as adapted for testing with CGCM results in section 4. Two methods of fitting the recharge oscillator to CGCM results are presented in section 5. These consist of either (i) fitting the models in their simplest, most condensed form, or (ii) fitting each of the physical balances from which the models are derived, and then combining them to examine the implied period. Because the simple model has considerable misfit with the CGCM results, we examine the improvements resulting from a modification to the model that permits an additional spinup time in wind stress, following Syu and Neelin (2000). The SSBH delayed oscillator model is presented in section 6 in a form that makes it highly comparable to the JIN97 model. A fitting by two exactly analogous methods is carried out in section 7, followed by a demonstration of the improvements resulting from the additional spinup time in wind stress. The implications of the problems encountered by the simple models in attempting to account for the CGCM data are discussed in section 8. We will argue that, for realistic ENSO variability, the framework of both the delayed oscillator and recharge oscillator models can be made substantially more complete by including coupled atmosphere–ocean mixed layer pro-

cesses. Having cast the models into comparable form in sections 5 and 6, and estimated their coefficients in a realistic regime, allows us to comment on their differences, or lack thereof, for practical purposes.

2. Model and simulation

The CGCM used in this study consists of the UCLA global atmospheric GCM (AGCM; Mechoso et al. 2000, and references therein) and the oceanic GCM (OGCM) known as Geophysical Fluid Dynamics Laboratory (GFDL) Modular Ocean Model (MOM; Bryan 1969; Cox 1984; Pacanowski et al. 1991). The AGCM has 15 layers in the vertical (with the top at 1 mb) and a horizontal resolution of 4° latitude by 5° longitude. MOM's domain is from 30°S to 50°N, and from 130°E to 70°W. The model has 27 layers in the vertical with 10-m resolution in the upper 100 m. The ocean has a constant depth of about 4150 m. The longitudinal resolution is 1°, the latitudinal resolution varies gradually from 1/3° between 10°S and 10°N to almost 3° at 50°N. A time-varying climatology is used to prescribe the SSTs outside the OGCM domain. No ad hoc corrections are applied to the information exchanged by model components. The model was integrated for 53 simulated years. The reader is referred to YM01 for further details on the model and simulation.

3. The simulated ENSO cycle

Figure 1 shows the time evolution of simulated SST and ocean heat content anomalies in the equatorial band between 4°S and 4°N. Here, ocean heat content is obtained by averaging ocean temperature in the upper 300 m. Anomalies are defined as the departures from the mean annual cycle. A low-pass filter was applied to the anomalies to remove the variability with timescales shorter than 1 yr. Figure 1a shows that anomalous warm SST events are produced approximately every 3–5 yr. Strong SST anomalies (up to 2°C) are simulated in the eastern to central Pacific, with peak strength around 150°W. All major warm SST events are associated with strong westerly wind stress anomalies to the west of the maximum SST anomalies, with maximum amplitudes close to 0.02 dyn cm^{-2} (see Fig. 2 in YM01). Figure 1b shows that ocean heat content anomalies with large magnitude and positive (negative) sign in the western Pacific tend to precede warm (cold) SST events in the eastern Pacific.

YM01 examines the correlative relationships between atmospheric and oceanic anomalies during the ENSO cycle by applying the M-SSA method to the SST, zonal and meridional components of surface wind stress, net surface heat flux, and ocean heat content. Two-dimensional latitude–longitude fields are taken in the 20°S–20°N latitudinal band in order to consider the possibility that the underlying dynamics of the cycle involves both the equatorial and off-equatorial Pacific (see YM01 for further details on the M-SSA application procedure.) The first pair of eigenvectors produced by the M-SSA represents an oscillatory mode that explains 23% of the variance in the combined variables and has a dominant period of about 48 months. This is very close to the simulated reoccurrence timescale of the ENSO-like SST anomalies by the CGCM. The eigenvector structures along the equatorial Pacific are displayed in Fig. 2 for ocean heat content, SST, and zonal wind stress anomalies. Figures 5, 6, and 7 in YM01 provide a more detailed picture of the atmospheric and oceanic structures of this mode. As summarized in Fig. 2, the simulated ENSO cycle is characterized by predominantly standing oscillations of SST in the eastern Pacific. Almost (though not quite) simultaneous zonal wind stress anomalies occur to the west of the SST anomalies. Thermocline anomalies in the east of the basin lead SST by a small amount and are in turn preceded by thermocline anomalies in the western part of the basin. These relationships are consistent with observations (Neelin et al. 1994) and with the general theoretical picture of an oscillation characterized by subsurface memory. The CGCM ENSO cycle thus appears qualitatively in keeping with both the JIN97 recharge oscillator model and the SSBH delayed oscillator model and provides a suitable testbed for addressing the questions raised in the introduction.

4. The recharge oscillator

In this section we briefly review the recharge oscillator model. In the onset of the peak stage, a positive SST anomaly induces a westerly wind stress anomaly at the equator. This has two effects. First, it sets up an anomalous slope of the equatorial thermocline with a magnitude that is proportional to wind stress. Second, it induces a divergence of the oceanic Sverdrup transport at the equator, which leads to a gradual reduction in zonal-mean thermocline depth. The first effect leads to a deepening of the thermocline in the eastern part of the basin, which participates in the positive feedback with SST and wind stress described in the Bjerknes hypothesis, eventually bringing the oscillation to the peak phase in SST. As this ends, the zonal-mean equatorial thermocline is shallowest. Climatological upwelling and the anomalies in subsurface temperature produced by shallow thermocline in the eastern part of the basin result in (i) an SST anomaly developing there, which induces an easterly wind stress anomaly; (ii) a deepening of the thermocline in the west; and (iii) a gradual increase of the mean thermocline depth (charge). The recharge oscillator sets out to produce a simple set of equations that link anomalies in SST variations, thermocline depth adjustment, and wind stress at the equator. The delayed oscillator attempts to do very much the same, but, because of the way it has been normally been formulated, we have found it simpler to

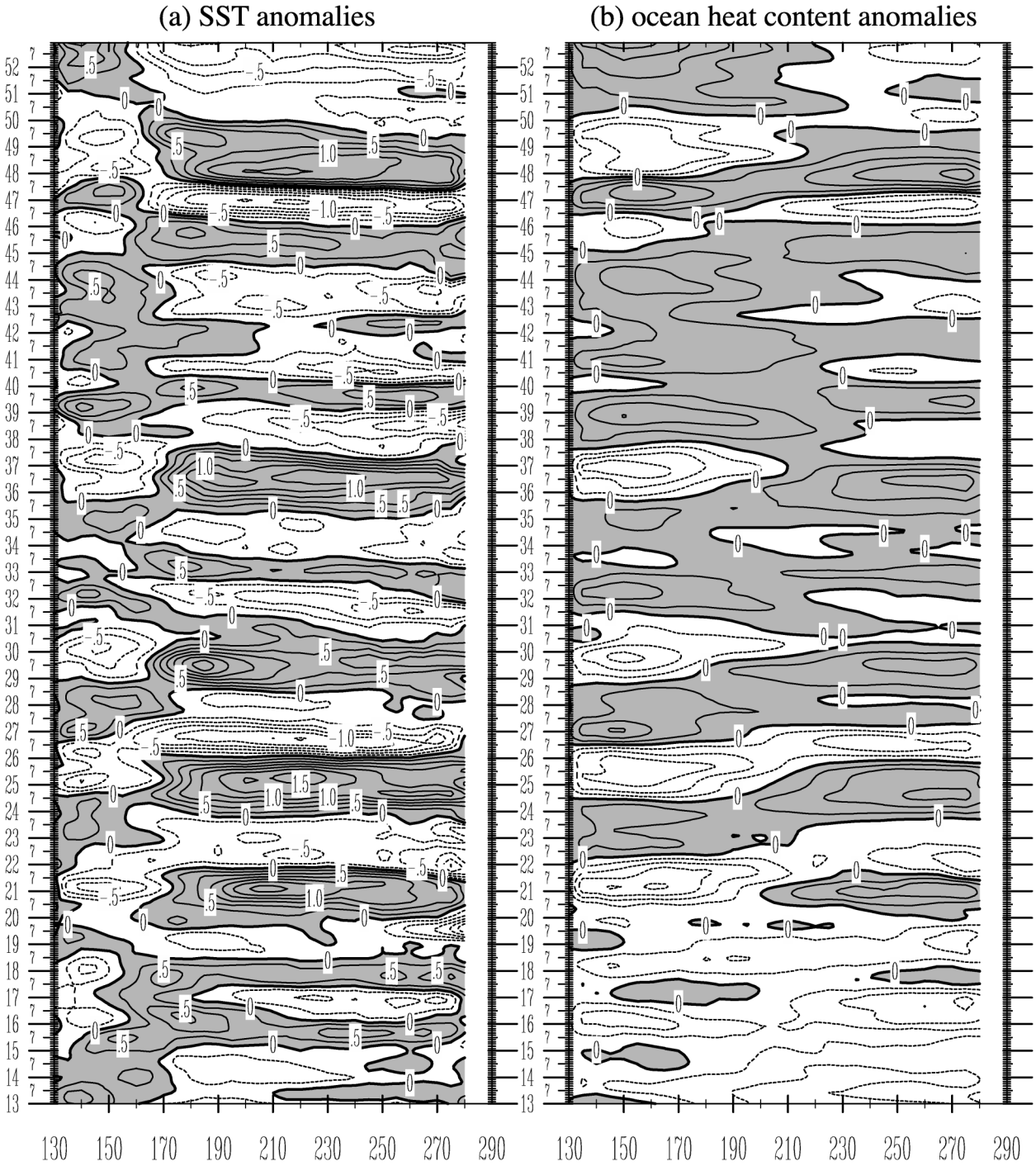

FIG. 1. Longitude–time cross sections of the simulated (a) SST and (b) ocean heat content and anomalies from the 53-yr CGCM simulation of Yu and Mechoso (2001). Anomalies from years 13 to 52 are shown. Annual cycles are removed. A low-pass filter is applied to remove anomalies with timescales shorter than 1 yr. Contour intervals are (a) 0.25°C and (b) 0.025 dyn cm^{-2}. Positive values are shaded.

spell out the steps for the JIN97 model, and then show the analogous set for the SSBH model.

JIN97 starts by assuming that differences in thermocline depth anomaly between the equatorial eastern and western Pacific are in approximate balance with the zonally integrated wind stress across the basin along the equator, here expressed as a zonal mean across the basin ($[\tau]$). This hypothesis must be reformulated in the context of the CGCM, which includes pressure and temperature but not thermocline depth among its variables. Consider that in approximate balance at the equator, the zonal momentum equation integrated vertically in the

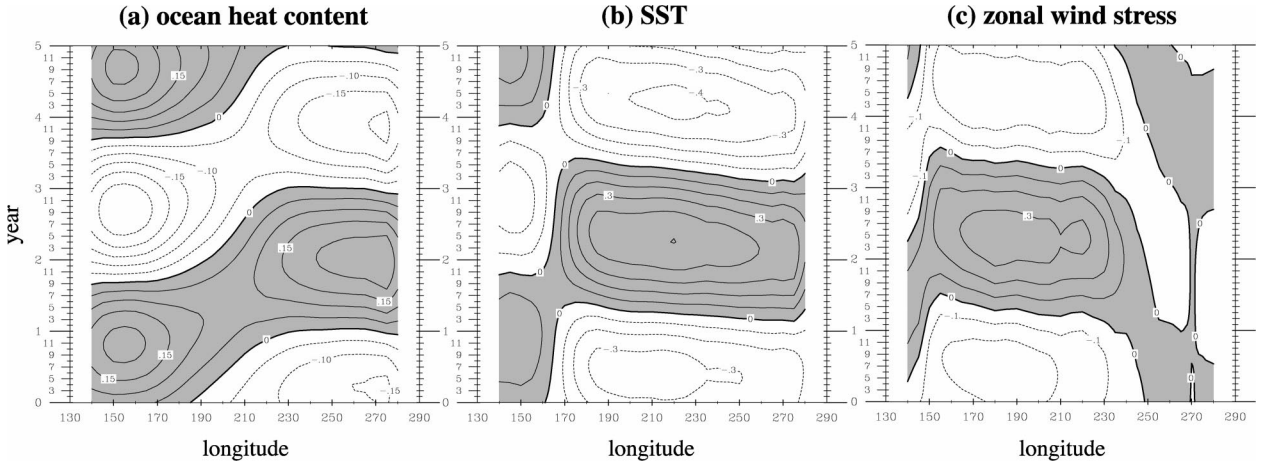

FIG. 2. The eigenvectors along the equatorial Pacific of the leading oscillation mode in the CGCM obtained from application of the combined five-variable M-SSA method (CGCM ENSO cycle): (a) ocean heat content, (b) SST, and (c) zonal wind stress anomalies. The vertical coordinate spans the 61-month window lag used in M-SSA. Contour intervals are (a) 0.05°C, (b) 0.10°C, and (c) 0.01 dyn cm^{-2}. Values shown in (c) are scaled by 10. Positive values are shaded. Panels (a), (b), and (c) are from Figs. 7a, 5a, and 5b, respectively, of Yu and Mechoso (2001).

upper 300 m of the ocean and from west (W) to east (E) gives

$$\left(\int_{-h}^{0} p\, dz\right)_E - \left(\int_{-h}^{0} p\, dz\right)_W = L[\tau], \tag{1}$$

where p is pressure, z is depth, $h = 300$ m, and L is the width of the basin. Use of the hydrostatic relationship yields

$$h[p_E(-h) - p_W(-h)] + g\int_{-h}^{0} (\rho_E - \rho_W) z\, dz = L[\tau], \tag{2}$$

which can also be written as

$$\int_{-h}^{0} (\rho_E - \rho_W)\left(1 + \frac{z}{h}\right) dz = L\frac{[\tau]}{gh}, \tag{3}$$

where the difference between surface pressure in the east and west was neglected. If salinity effects are neglected, then the equation of state can be approximated by

$$\rho = \rho_0[1 + \varepsilon(T - T_0)], \tag{4}$$

where ρ_0, T_0, and ε are constant. Therefore,

$$\frac{1}{h}\int_{-h}^{0} T_E\left(1 + \frac{z}{h}\right) dz = \frac{1}{h}\int_{-h}^{0} T_W\left(1 + \frac{z}{h}\right) dz + L\frac{[\tau]}{\rho_0 \varepsilon g h^2}. \tag{5}$$

In view of (5), we reformulate the starting hypothesis in JIN97 in the following way:

$$\frac{1}{\lambda K_E} H_E = \frac{1}{\lambda K_W} H_W + [\tau], \tag{6}$$

where H_E and H_W are the upper-ocean heat content anomalies in the equatorial eastern and western Pacific, respectively, and the coefficients K_E, K_W, and λ are assumed to be constant.

JIN97 (and other simple models) also postulate that the wind stress anomalies along the equator and SST anomalies in the eastern part of the ocean satisfy a linear relationship. For the zonal-mean wind stress this requires

$$[\tau] = bT_E, \tag{7}$$

where b is constant.

In the remainder of this paper we rewrite the expressions in JIN97 by replacing thermocline depth with upper ocean heat content. The first of the two prognostic equations in the recharge oscillator model states that the equatorial adjustment process can be described by

$$\frac{dH_W}{dt} = -rH_W - \alpha[\tau], \tag{8}$$

where the first term of the right-hand side represents ocean adjustment processes that are assumed to act at a constant rate r, and the second term represents the Sverdrup transport across the basin. This equation is only heuristically justified, but is intended to capture the overall effect of oceanic adjustment processes (including the net effect of Rossby wave adjustment). Substitution of (7) in (8) gives

$$\frac{dH_W}{dt} = -rH_W - \alpha bT_E. \tag{9}$$

The second prognostic equation used in the recharge

oscillator model is based on the SST equation for a box in the eastern Pacific:

$$\frac{dT_E}{dt} = -cT_E + \gamma H_E, \tag{10}$$

where the first term in the right-hand side represents decay processes due to heat exchange between atmosphere and ocean that are assumed to act at a constant rate c, and the second term represents thermocline feedback processes mediated by upwelling. In the context of the CGCM, feedback processes associated with upwelling and zonal advection by surface layer currents can implicitly affect c, insofar as they have little time lag relative to wind stress anomalies and thus to SST anomalies.

Using (6) and (7) in (10), we obtain

$$\frac{dT_E}{dt} = RT_E + K_E K_W^{-1} \gamma H_W, \tag{11}$$

where the parameter

$$R = K_E \lambda b \gamma - c \tag{12}$$

represents the Bjerknes positive feedback process of tropical atmosphere–ocean interactions.

The oscillation equation is obtained from (9) and (11), which gives

$$\frac{d^2T_E}{dt^2} - (R - r)\frac{dT_E}{dt} + (K_E K_W^{-1} \alpha b \gamma - Rr)T_E = 0. \tag{13}$$

We note the importance of the combination of parameters $K_E K_W^{-1} \alpha b \gamma$, which is the leading effect tending to produce oscillatory behavior. Provided the solutions are oscillatory, the growth rate is given by $(R - r)/2$ and the period by

$$P = 2\pi[K_E K_W^{-1} \alpha b \gamma - (R^2 + r^2)/4]^{-1/2}. \tag{14}$$

5. Does the recharge oscillator fit the CGCM results?

Our approach in this section is to determine the coefficients of the equations in section 4 by least squares fitting to the CGCM ENSO cycle. To fit the simple model, we define variables from the CGCM based on the following averaging regions: H_W is upper ocean average temperature anomaly above 300 m, 4°N–4°S, 140°E–180°; H_E is upper ocean average temperature anomaly above 300 m, 4°N–4°S, 120°–80°W; T_E is the SST anomaly 4°N–4°S, 120°–80°W; and $[\tau]$ is the wind stress anomaly averaged across the Pacific from 130°E–70°W.

It is clear that with the available parameters, any oscillation frequency can be fit, so a test of the model must rely on fitting parameters in sets of the individual equations that make up the model. This procedure is nonunique. We contrast two methods.

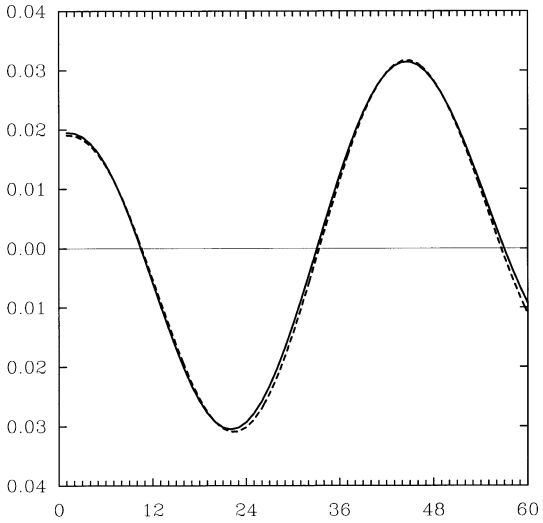

FIG. 3. The solid and dashed lines represent the left- and right-hand sides of Eq. (9), respectively, calculated from the CGCM simulation with $r = 0.108$ month K^{-1} and $\alpha b = 0.104$ month^{-1}.

- *Method 1*: Fitting the final pair of derived equations [(9) and (11)] with two unknowns, H_W and T_E.
- *Method 2*: Fitting the set of equations [(6), (7), (8), and (10)] corresponding to individual physical balances or approximations that led to the derivation. The CGCM variables used in this are H_W, T_E, H_E, and $[\tau]$.

In each case, amplitude information is relevant, as well as phase and period, since relations among oscillatory CGCM variables are examined. Furthermore, amplitude variation in the M-SSA modes contains some further information regarding how related variables covary.

We can anticipate that reproducing the period of the target oscillation by the fitting of method 1 will not be difficult since any two variables containing differing phase information can be used to characterize an oscillation. We also test method 1 by cross checking the implications of the resulting parameters in the equations of method 2. We can also anticipate that the growth rate will be more sensitive than the period when fitting a linear model to an equilibrated oscillation. We thus give the growth or decay rate primarily as a further indicator of sensitivity among the two methods and the two models.

a. Method 1 fitting

Figure 3 shows that the derived H_W Eq. (9) can give a good fit among CGCM values of dH_W/dt, H_W, and T_E with

$$r = 0.108 \text{ month}^{-1}; \qquad \alpha b = 0.104 \text{ month}^{-1}. \tag{15}$$

Figure 4 shows that (11) gives a reasonable fit among dT_E/dt, T_E, and H_W for

$$R = 0.0988 \text{ month}^{-1};$$
$$K_E K_W^{-1} \gamma = 0.269 \text{ month}^{-1}. \tag{16}$$

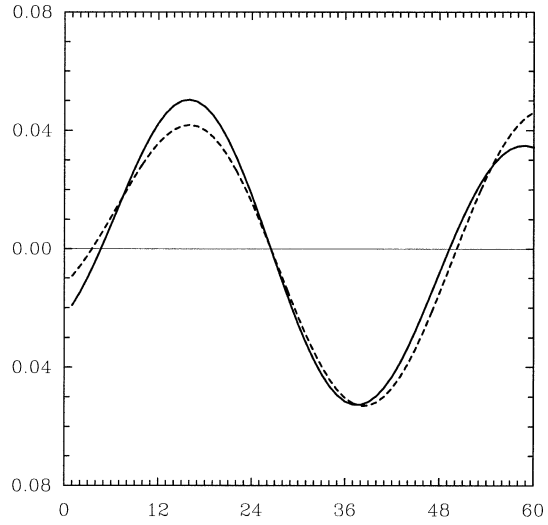

FIG. 4. The solid lines represent the left- and right-hand sides of Eq. (11), respectively, calculated from the CGCM simulation with $R = 0.0988$ month^{-1} and $K_E K_W^{-1}\gamma = 0.269$ month^{-1}.

These values yield a period of 4.0 yr. and a slow *decay* rate of (9 yr)$^{-1}$ consistent with our expectations. Were this the only calculation performed, one might be tempted to conclude that the recharge oscillator provides a reasonable fit to the CGCM results.

b. Method 2 fitting

Figure 5 shows the fitting of (6), the equatorial pressure gradient relation. The procedure provides a good fit among H_E, H_W, and $[\tau]$ for

$$K_E\lambda = 16.6 \text{ dyn}^{-1} \text{ cm}^2 \text{ K};$$
$$K_W\lambda = 28.2 \text{ dyn}^{-1} \text{ cm}^2 \text{ K}. \quad (17)$$

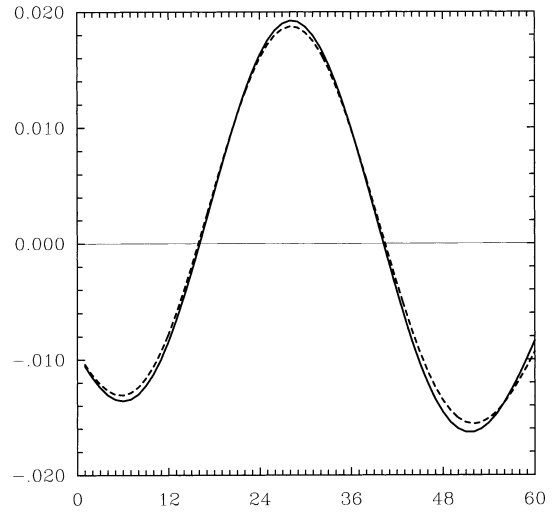

FIG. 5. The solid and dashed lines represent the left- and right-hand sides of Eq. (6), respectively, calculated from the CGCM simulation with $\lambda K_E = 16.6$ dyn^{-1} cm^2 K and $\lambda K_W = 28.2$ dyn^{-1} cm^2 K.

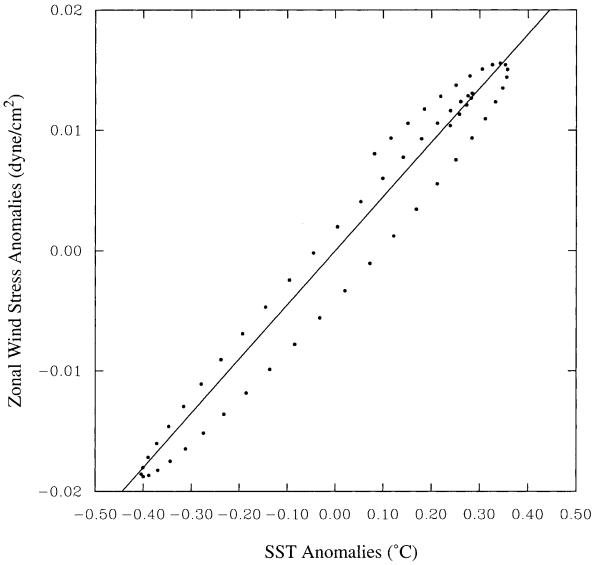

FIG. 6. Scatterplot for zonal wind stress ($[\tau]$) and SST (T_E) anomalies of the CGCM ENSO cycle. The straight line represents $[\tau] = bT_E$, with $b = 0.045$ dyn cm^{-2} K^{-1}.

The different values of K_E and K_W reflect the different density structures in the eastern and western Pacific. Figure 6 shows the relation between wind stress and SST anomalies, implying that (7) holds very approximately for

$$b = 0.045 \text{ dyn}^{-1} \text{ cm}^2 \text{ K}^{-1}. \quad (18)$$

Turning to (8), the original postulate for dH_W/dt, as opposed to (9) used in method 1, Fig. 7 shows a very reasonable fit of dH_W/dt on H_W and $[\tau]$ for

$$r = 0.161 \text{ month}^{-1};$$
$$\alpha = 2.77 \text{ dyn}^{-1} \text{ cm}^2 \text{ month}^{-1} \text{ K}. \quad (19)$$

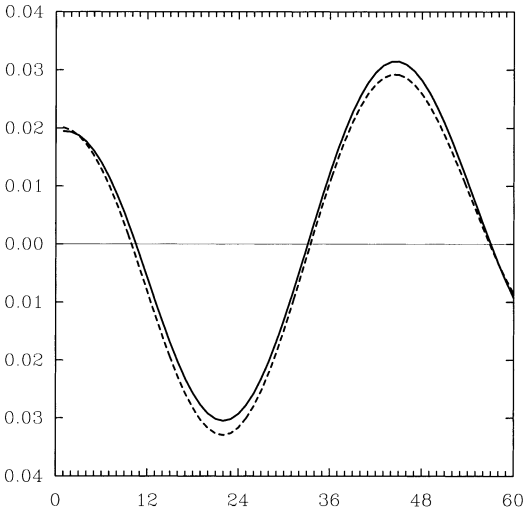

FIG. 7. The solid and dashed lines represent the left- and right-hand sides of Eq. (8), respectively, calculated from the CGCM with $r = 0.161$ month^{-1} K and $\alpha = 2.77$ dyn^{-1} cm^2 K.

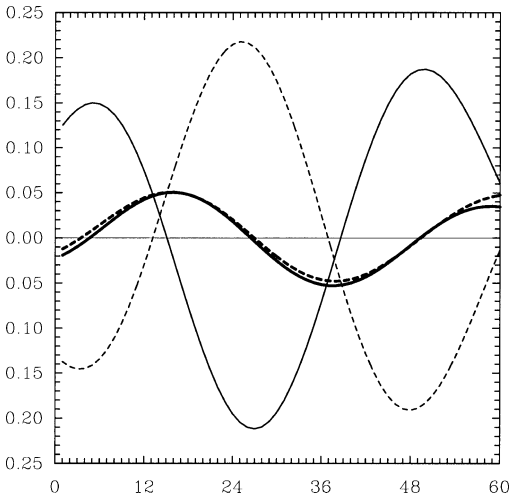

FIG. 8. The thin-solid and dashed lines represent the left- and right-hand sides of Eq. (10), respectively, calculated from the CGCM simulation with $c = 0.524$ month^{-1} and $\gamma = 0.999$ month^{-1}. The thick-solid and thin-dashed lines represent the $-cT_E$ and γH_W terms on the right-hand side of Eq. (10), respectively.

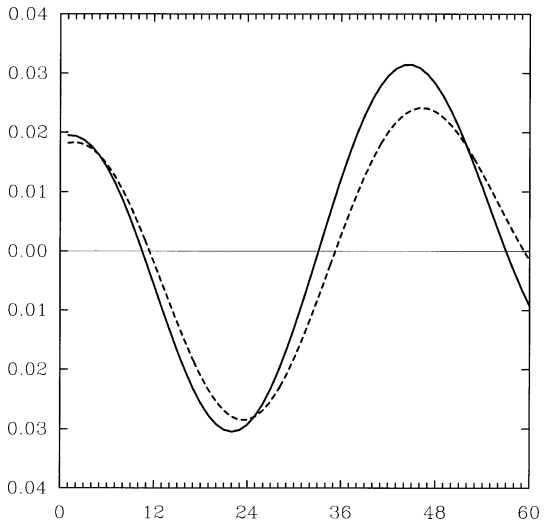

FIG. 9. The solid and dashed lines represent the left- and right-hand sides of Eq. (8), respectively, calculated from the CGCM simulation with $r = 0.108$ K month^{-1} and $\alpha = 2.31$ dyn^{-1} cm^2 K as estimated by method 1. Contrast with Fig. 7, which is obtained using the values of r and α estimated by method 2.

Finally, using (10), the original form of the dT_E/dt equation, and fitting on T_E and H_E yields

$$c = 0.524 \text{ month}^{-1}; \qquad \gamma = 0.999 \text{ month}^{-1}. \quad (20)$$

Figure 8 shows that this fit holds fairly well. Also shown are curves corresponding to the individual contributions $-cT_E$ and γH_E. These cancel to a large degree, but H_E leads T_E by about 2 months (consistent with the value of c). Such a lead is due to the time it takes the surface layer to warm, determined by its heat capacity compared to the strength of upwelling processes. Though relatively small, the lead is essential to the oscillation. If the approximation $T_E = c^{-1}\gamma H_E$ were used, the JIN97 model would not oscillate.

For comparison to method 1, the c, b, $K_E\lambda$, and γ values imply from (12)

$$R = 0.222 \text{ month}^{-1}, \quad (21)$$

while $K_E K_W^{-1}\gamma = 0.588$ month^{-1} and $\alpha b = 0.124$ month^{-1}. The resulting period is 2.7 yr and the *growth* rate (2.7 yr)$^{-1}$. Thus, fitting the model in a manner that tests the hypothesized physics step by step results in very substantial differences in parameters. The period is actually a poorer fit to that of the CGCM. The primary contribution to the difference in period comes from fitting γ separately from K_E and K_W rather than fitting the product used in method 1.

c. Cross-checking method 1 fitting in method 2

As a means of visualizing the allocation of errors in the different fitting processes, we take coefficients from fitting the two prognostic equations in method 1 and substitute them into the two prognostic equations in method 2. Since method 1 produces lumped combinations of parameters, we use the values determined from the diagnostic equations in method 2 where needed. We have also performed the reverse operation and the information content is very similar (not shown).

Figure 9 shows the results for the original dH_W/dt equation using r and αb given by method 1 in (15), which directly provides the former parameter and that yields $\alpha = 2.31$ dyn^{-1} cm^2 month^{-1} K with (18). Substantial errors in amplitude and, to a lesser extent, in phase are implied in the original equation. The fitting process in the derived Eq. (9) has produced parameters that are less faithful to the postulated physics in an effort to compensate for some inherent error in the simple model.

Figure 10 shows the results for the dT_E/dt equation using c and γ given by (16) of method 1 with (17) and (12). These values ($c = 0.244$ month^{-1}; $\gamma = 0.480$ month^{-1}) are less than half of those estimated in method 2 in (20). Compared to dT_E/dt from the CGCM, the phase is well reproduced, but the amplitude is roughly half of what it should be. Again, the fitting in method 1 has been more faithful to the period of the oscillation than to the parameters in the underlying physical balances. It appears that both Eqs. (9) and (11) of the JIN97 model contribute to the error.

d. Sensitivity to choice of averaging region

In order to evaluate the sensitivity of the results to the choice of eastern, western, and wind stress averaging regions, we repeated our calculations using the following regions: eastern region for H_E and T_E, where H_E is 150°–80°W; western region for H_W, where T_W is 140°E–150°W; and wind stress region is 160°E–120°W in the

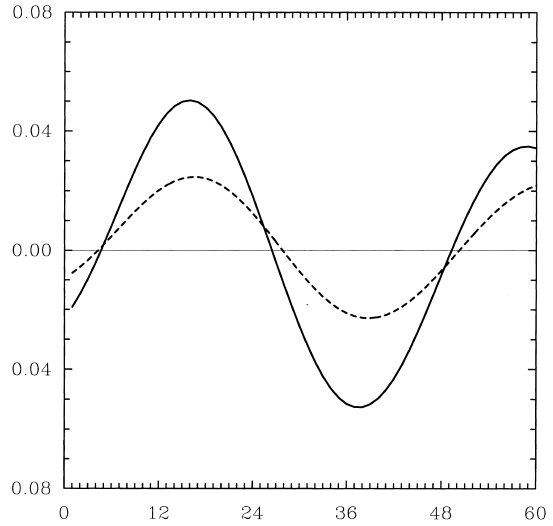

FIG. 10. The solid and dashed lines represent the left- and right-hand sides of Eq. (10), respectively, calculated from the CGCM simulation with $c = 0.244$ month^{-1} and $\gamma = 0.480$ month^{-1}, as estimated by method 1. Contrast with Fig. 8, which is obtained using the values of c and γ estimated by method 2.

western-central Pacific straddling the two thermodynamic regions. This variant is closer to a two-box model with no gap between the eastern and western regions; also, the eastern region is considerably longer. As a result, some of the individual parameters estimated from the fitting change noticeably. For method 1 fitting, the values in (15) and (16) become $r = 0.091$ month^{-1}, $\alpha b = 0.069\ 56$ month^{-1}; $R = 0.0986$ month^{-1}, and $K_E K_W^{-1}\gamma = 0.385$ month^{-1}. The values of αb and $K_E K_W^{-1}\gamma$ each change by about 30% but in a manner that compensates, as expected for method 1, so that the period is almost unchanged. The implied growth rate is slightly smaller than the already small value previously obtained, with a growth time of 22 yr.

For method 2, (17), (18), and (19) become $K_E\lambda = 8.4$ dyn^{-1} cm^2 K, $K_W\lambda = 12.2$ dyn^{-1} cm^2 K, $b = 0.067$ dyn^{-1} cm^2 K, $r = 0.127$ month^{-1}, and $\alpha = 1.118$ dyn^{-1} cm^2 month^{-1} K. These considerable changes in the individual parameters also tend to have canceling effects on the period which, although it increases to 3.3 yr, remains considerably shorter than in the CGCM (4 yr). The growth time increases to 4.7 yr.

This sensitivity test implies caution regarding the individual values of the parameters, but suggests an overall robustness of the conclusions regarding the period. Again, the simple model does not fully capture the period when required to satisfy the individual physical balances.

e. Modified atmospheric model

The behavior of the basin-mean wind stress displayed in Fig. 6 departs systematically from a simple proportionality to T_E. As the SST anomaly increases, the wind stress follows more slowly than the linear fit, and vice versa during the decreasing phase. This suggests that the wind stress may be adjusting toward SST with a finite adjustment time on the order of a month or more. While this is short compared to the ENSO period, Syu and Neelin (2000) and Neelin et al. (2000) found that this could make a noticeable difference to the ENSO period. The former authors proposed a simple extension of steady atmospheric models to take this effect into account. Instead of (5), they use

$$[\tau] = b\frac{1}{\eta}\int_{-\infty}^{t} T_E(t - s)e^{-s/\eta}\, ds, \tag{22}$$

where η is the adjustment timescale of the atmosphere, here approximated as an exponential adjustment toward equilibrium with SST. As $\eta \to 0$, the original steady atmosphere (5) is recovered.

Figure 11 shows the values obtained from (22) using $\eta = 2.5$ month, with $b = 0.40$ dyn cm^{-2} K^{-1} slightly adjusted as well for a best fit (minimized least square error). The modified atmosphere captures leading aspects of the departure from a linear relation (cf. Figs. 11 and 6), although the apparent adjustment time in the CGCM differs somewhat during SST decreasing and increasing phases. The orbit passes closer to the linear fit during decreasing SST phase in the CGCM suggesting a slightly smaller adjustment time. We note that the adjustment time in the CGCM need not be purely atmospheric. Atmospheric wave adjustment interacting with moist processes does have a timescale potentially on the order of a month or more, but the best-fit value of 2.5 months is on the long side. Interaction with the ocean surface layer in regions outside the eastern Pacific equatorial cold tongue could contribute. It is also possible that the slight westward propagation seen in the CGCM SST anomalies (see Fig. 5 in YM01) may contribute to this effect. In this case, it would be largely an ocean surface layer process contributing to the memory of the coupled oscillation.

For an oscillation of the form $T_E e^{i\omega t}$ (ω may be complex), the modified atmosphere model yields

$$[\tau] = bT_E(1 - i\omega\eta)^{-1}e^{i\omega t}. \tag{23}$$

This expression may be manipulated to show that the effect of the adjustment time is equivalent to a frequency-dependent reduction of amplitude that damps higher frequencies combined with a lag of approximately η (for $\omega\eta$ small). We underline that the effect of the adjustment time is substantially different than would be a lag representation.

We now consider the impact on the period of the JIN97 model. Equation (8) becomes

$$(i\omega + r)H_W = -\alpha bT_E(1 + i\omega\eta)^{-1}, \tag{24}$$

and the dispersion relation derived from (13) is modified to

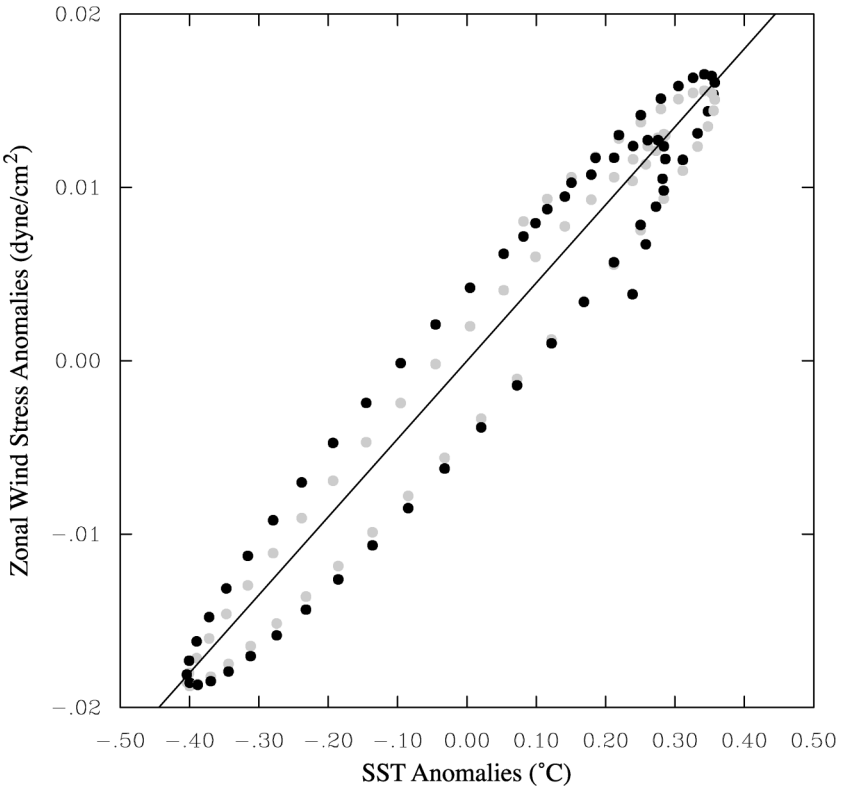

FIG. 11. Scatterplot for zonal wind stress ($[\tau]$) and SST (T_E) anomalies of the CGCM ENSO cycle. Dark points are for zonal wind stress ($[\tau]$) anomalies estimated by the modified atmospheric model of Eq. (25) using the simulated SST anomalies (T_E). Gray points and the line are from those of Fig. 6.

$$\omega^2 + [K_E\lambda\gamma b(1 + i\omega\eta)^{-1} - c - r]i\omega - (K_E K_W^{-1}\gamma\alpha b - K_E\lambda\gamma br)(1 + i\omega\eta)^{-1} - cr = 0. \quad (25)$$

Here, the parameter R defined in (12) is no longer relevant because it arose by eliminating H_E using (6) and the modified atmosphere affects the wind stress in (6).

Using the parameter values from method 2, with η and b values derived above, yields a *growth* rate of (2.2 yr)$^{-1}$ and a period of 4.2 yr. Thus the atmospheric adjustment time, though small, has a large effect. It improves the period reproduced by the model very substantially relative to the JIN97 model alone, which had a period of only 2.7 yr. The modified model also captures to a reasonable approximation the elliptical orbit seen in the $[\tau]$–T_E plane in Figs. 6 and 11.

6. The delayed oscillator model

The delayed oscillator model can be written in a form very closely related to the recharge oscillator. The T_E equation (10), the equatorial pressure gradient equation (6), and the atmospheric equation (7) remain the same. The H_W equation is altered, replacing (9) with

$$H_W = -\alpha^*[\tau(t - \delta)], \quad (26)$$

where δ is the delay time. We use zonal average stress because the difference $H_E - H_W$ depends on the zonal average across the basin. In the SSBH model, wind stress is assumed to be highly localized to give a discrete lag. In the CGCM, the lag must be interpreted as a weighted mean Rossby wave travel time, that is, the average of the wind stress anomaly at each point times the distance from the western boundary times the Rossby wave speed. The equatorial pressure gradient equation (6) assumes that the crossing time of the Kelvin wave is rapid compared to the Rossby wave adjustment. This should set a good approximation (see Neelin et al. 1998) and it permits the point-coupling assumption of the delayed oscillator to be relaxed in the very important east–west gradient. In the CGCM, Eq. (6) holds very well as seen in Fig. 5.

Combining (26) with (7) gives

$$H_W = -\alpha^* bT_E(t - \delta). \quad (27)$$

With (11), this gives a pair of equations with strong parallels to the JIN97 model. We can also make use of the set of equations prior to elimination to give a system similar to that estimated in method 2 in section 5.

Combining (27) with (11) leads to the familiar form of the SSBH delayed oscillator

$$dT_E/dt = RT_E - K_E K_W^{-1}\gamma\alpha^* bT_E(t - \delta). \quad (28)$$

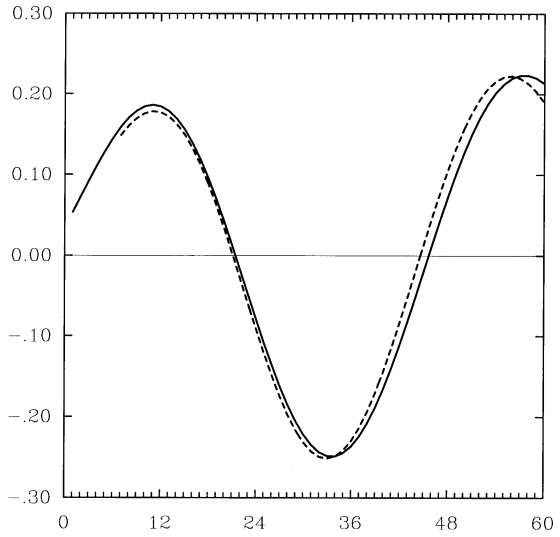

FIG. 12. The solid and dashed lines represent the left- and right-hand sides of Eq. (27), respectively, with $\alpha^* b = 0.622$ and $\delta = 6.0$ month.

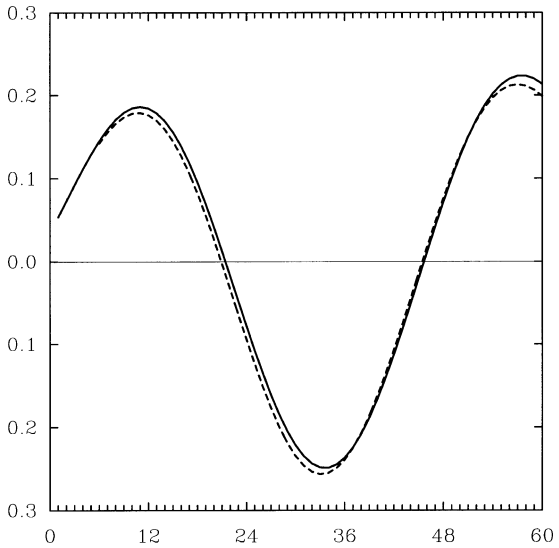

FIG. 13. The solid and dashed lines represent the left- and right-hand sides of Eq. (26), respectively, with $\alpha^* = 13.7$ dyn^{-1} cm^{-2} K and $\delta = 5.0$ month.

For oscillations of the form $\exp[i\omega t]$, the dispersion relation becomes

$$(i\omega - R) = -K_E K_W^{-1} \gamma \alpha^* b \exp[-i\omega\delta]. \qquad (29)$$

7. Does the SSBH delayed oscillator fit the CGCM results?

As for the recharge oscillator, we can fit the model in either more reduced form, in which case the physical parameters are lumped into a smaller set, or it can be fit at the level of the individual physical balances. These choices lead, respectively, to method 1 and method 2 parallel to those used in the JIN97 case.

a. Method 1 fitting

Figure 12 shows the fit for H_W on lagged T_E following the combined Eq. (27), leading to values for $\alpha^* b = 0.622$ and $\delta = 6.0$ month (least squares fitting for $\alpha^* b$ was used for a sequence of values of δ and the value giving the minimum square error was chosen). Using the values $R = 0.0998$ month^{-1} and $K_E K_W^{-1} \gamma = 0.2695$ month^{-1} as estimated in (16) for method 1 of section 5, leads to a period of 3.5 yr and a decay rate of (3.9 yr)$^{-1}$. Compared to the CGCM oscillation period of 4.0 yr, the method 1 fitting yields a slightly less exact fit for the delayed oscillator than the JIN97 model. Sensitivity studies suggest the period is slightly more sensitive to parameters than the JIN97 model, but this still does not appear to account fully for the misfit. For instance, a value of $\delta = 6.0$ month yields a period of 3.7 yr. Nonetheless, method 1 still appears to overfit the model parameters when we turn to the more detailed evaluation of the model in method 2.

b. Method 2 fitting

Figure 13 shows the best fit for H_W on lagged wind stress, leading to values of $\alpha = 13.7$ dyn^{-1} cm^2 K and $\delta = 5$ month. Using $b = 0.045$ dyn cm^{-2} K^{-1}, as obtained in (18), $K_E K_W^{-1} \gamma \alpha b = 0.183$ month^{-1}. The fitting of the T_E equation is the same as in section 5, method 2. Again we note that the 2-month lag between T_E and H_E, though small, is important to the oscillation; the time derivative of T_E cannot be ignored. With $R = 0.2218$ month^{-1} from (21), the period predicted by the SSBH model is 2.7 yr and the *growth* rate is (0.9 yr)$^{-1}$. The period is essentially the same as was predicted by the JIN97 model for method 2. Thus it appears that both models are missing some important ingredient in the dynamics of the CGCM.

Battisti and Hirst (1989) carried out a detailed fitting procedure of the SSBH model to the Battisti (1988) version of the Cane and Zebiak (1985) model. We can compare results to their fitting for the period and the following combinations of parameters: R defined by (12) compares to the parameter they called b, and $K_E K_W^{-1} \alpha b \gamma$ compares to the parameter they called c. Their standard values were, respectively, 0.18 and 0.325 month^{-1}, while their delay time was 6 months. Using these in (29) gives a period of 3.0 yr (when ad hoc nonlinear terms were included in their calculation they resulted in a slightly shorter period—about 2.6 yr). The Battisti and Hirst (1989) parameters are of the same order of magnitude as those in the CGCM, but differ by almost a factor of 2 for $K_E K_W^{-1} \gamma \alpha b$, which is somewhat compensated by the differences in the other parameters in their effects on period. This comparison suggests qualitative similarity but quantitative differences between

the CGCM and the Battisti (1988) intermediate model for the processes that the SSBH model does capture.

c. Modified atmospheric model

We again turn to the modified atmosphere to examine whether the misfits can be reduced. The dispersion relation for the SSBH model with the atmosphere modified according to (23) is

$$\{i\omega - [K_E\lambda\gamma b(1 + i\omega\eta)^{-1} - c]\} = -K_E K_W^{-1}\gamma\alpha b(1 + i\omega\eta)^{-1}\exp[-i\omega\delta]. \quad (30)$$

Using the values of $\alpha = 13.7$ dyn^{-1} cm^2 K and $\delta = 5$ month obtained by method 2 above, with values for c and γ given by method 2 in (20), and with values for $\eta = 2.5$ month and $b = 0.40$ dyn cm^{-2} K^{-1} from the modified atmosphere fitting in section 5d, we obtain a period from (30) of 3.6 yr and a *decay* rate of (1.3 yr)$^{-1}$. As in the JIN97 model, although to a lesser extent, including the modified atmosphere in the SSBH model substantially improves the predicted period.

8. Summary and discussion

We use a realistic 53-yr-long CGCM simulation analyzed in YM01 to examine two conceptual models of ENSO—the JIN97 model, also known as the recharge oscillator, and the SSBH delayed oscillator model. The questions raised refer to the completeness of ENSO depiction provided by those models and their relative validity. To provide a consistent target for the simple models, the CGCM results are prefiltered with a multichannel singular spectrum analysis. The leading oscillatory mode captured by the M-SSA (CGCM ENSO cycle) resembles in many aspects the observed ENSO cycle. In particular, it is characterized by predominantly standing oscillations of SST anomalies in the eastern Pacific, almost simultaneous zonal wind stress anomalies to the west of the SST anomalies, and preceding thermocline anomalies in the west of the basin.

Two methods are used to fit the simple models to the CGCM. In its simplest form, the JIN97 model can be reduced to two ordinary differential equations, one for equatorial eastern Pacific SST T_E and one for equatorial western Pacific heat content H_W. The SSBH model can be expressed with the same equation for T_E, and a delay equation for H_W. Fitting parameters of the simple models in such a reduced form is referred to as method 1. This is not a stringent test; for instance, a purely empirically motivated oscillator equation or second-order autoregressive process could be fit to the period of the CGCM equation. The method 1 fitting can yield an oscillation as long as the two included variables, in this case equatorial eastern Pacific SST and western Pacific heat content, have sufficient phase difference. The method does require that the chosen parameters reproduce phase and amplitude relations among these two variables and then that these parameters yield the correct period (and furthermore the amplitude variation within the M-SSA oscillation provides some degree of further test). The simple models can instead be fit using the individual physical balances that are used to derive them, referred to as method 2. The equation for T_E is has a dependence on equatorial eastern Pacific heat content, the pressure gradient relation across the equator links this to wind stress and to H_W, the equation for H_W is expressed in terms of wind stress in both models, and a linear atmospheric model links wind stress to T_E. The method 2 fitting thus requires the parameters of the simple model to reproduce amplitude and phase relationships among four variables derived from the CGCM and then to predict a period for comparison to the CGCM.

Some of the caveats on the present approach to testing simple models include the following. The simple models are treated in linear form, whereas the CGCM oscillation is a finite amplitude oscillation. It is known from a variety of intermediate model studies (Battisti and Hirst 1989; Jin and Neelin 1993; Jin et al. 1996) that while the linear period captures the finite amplitude period to a first approximation, nonlinear processes and noise can modify (often increase) the period. The period is much less sensitive than the growth rate, since the first effect of the nonlinearity is simply to balance the growth rate if the mode is unstable. If the mode is stable, then the balance is between decay rate and stochastic input from the atmosphere. Further, we do not carry out the Floquet theory to evaluate impacts of the seasonal cycle on the mode, although these are modest for period (Jin et al. 1996). With this in mind we do not attempt to conclude anything about the maintenance of the mode from the simple models, and draw conclusions only when discrepancies in the period are large. On the other hand, one might argue that a fitting procedure is rather too favorable to the simple models, since we determine the parameters that provide the best fit to the CGCM output rather than estimating a priori. Linear empirical models have been shown to fit ENSO time series (Penland and Magorian 1993; Jiang et al. 1995; Burgers 1999; Thompson and Battisti 2000) in tests (including irregularity, spectral characteristics, and predictive capability) more demanding than posed here. This suggests a negative outcome for the simple model may be a more reliable outcome than a positive one.

Using the method 1 fitting, the JIN97 model reproduces the period of the CGCM oscillatory mode accurately. The SSBH model fit by method 1 yields a period of 3.5 yr, somewhat off from the period of 4.0 yr of the CGCM mode. This is possibly due to the slightly greater sensitivity of the SSBH model to parameters. If one were only to use method 1, one might be misled into concluding that the simple models reproduced the CGCM oscillation reasonably well. However, when the parameters implied by the method 1 fitting were substituted into the physical balances of method 2 in a cross-checking procedure, they were found to

yield substantial errors in the amplitude (and to a lesser degree, the phase) of the relationships among CGCM variables.

Using method 2 the period predicted by both the JIN97 and SSBH models is only 2.7 yr, clearly a poor fit to the CGCM period. A sensitivity test changing the averaging regions in an attempt to improve model fit was only able to increase the period predicted by JIN97 to 3.3 yr, which is still shorter than the CGCM. We caution that the mismatch of period alone would not necessarily prove that there is missing physics in simple models. Clear evidence of at least one nonincluded process is given by time-dependent behavior of CGCM anomalies of wind stress and SST: plots of the former versus the latter show orbits where the wind stress increases and decreases more slowly than the SST. The physics for such behavior is neglected in the both SSBH and JIN97 models, but the question is whether this omission is significant.

To account for such time-dependent behavior we introduced, in both the JIN97 and SSHB models, the atmospheric adjustment time model of Syu and Neelin (2000). In this context, wind stress is represented as an integral over past SST, exponentially weighted with an adjustment time. For a small adjustment time, this model reduces to the linear relation between stress and SST anomalies used in the JIN97 and SSBH models. Fitting to the CGCM results yields an adjustment time of 2.5 months, which reproduces the phase plane orbit quite well. From Syu and Neelin (2000) and Neelin et al. (2000), it is known that such an adjustment time, though short, can increase the period of ENSO models. A very substantial increase in period is indeed found when this modified atmosphere is added to both the recharge oscillator and the delayed oscillator model. In the former, the period increases from 2.7 to 4.2 yr; in the latter, from 2.7 to 3.6 yr. Sensitivity studies on the parameters suggest that this is a close enough fit to the actual period that we may presume that the main missing physics is associated with the adjustment time between equatorial wind stress and eastern equatorial SST anomalies. This adjustment time is long enough that we believe that it is not purely atmospheric, but rather involves ocean mixed layer processes outside the eastern equatorial Pacific, spinning up in conjunction with the atmosphere.

Our scenario for the missing physics is consistent with the behavior found in intermediate complexity models by Jin and Neelin (1993) and Dijkstra and Neelin (1995) for what the former authors referred to as mixed SST/ocean-dynamics mode (abbreviated as mixed mode below). The spatial structure is largely determined by Bjerknes hypothesis feedback as in an SST mode, and the subsurface adjustment processes represented as a lag in the SSBH model or an adjustment of H_W in the JIN97 model can produce and oscillatory tendency. Other adjustment processes, however, including coupled interactions between the atmosphere and the ocean surface mixed layer can easily modify the period. The need for additional physics before the simple models can mimic the CGCM illustrates how additional mechanisms can affect the ENSO mode for which there exist a number of observationally based indications (e.g., Wang et al. 1999; Weisberg et al. 1999).

Regarding growth or decay, the two models give relatively consistent results for each method: slow decay when estimated by method 1, growth when estimated by method 2, and decay at a timescale of 1–2 yr when the modified atmosphere is included. We do not regard the growth rate results as very trustworthy due to the sensitivity considerations outlined above. Nevertheless, the best-fitting cases (with the modified atmosphere) appear to agree with the concept that the ENSO oscillation is decaying and maintained by atmospheric noise (Blanke et al. 1997; Eckert and Latif 1997; Kleeman and Moore 1997).

Below we summarize the main conclusions (subject to the caveats discussed above).

1) An object lesson in the difficulty of verifying simple models is provided by method 1, which yields an apparent verification of the models that on closer examination turns out to be simply an overfitting. We recommend breaking simple models into their component hypotheses for verification. Method 2 provides an example of this procedure.
2) The two models are analyzed in a form where similarities between them in several physical balances are explicit. The one postulated balance that differs between the two—the relation of western Pacific heat content to wind stress—is fit separately and could potentially yield different results for the two models. However, when fit to CGCM results in the realistic regime, the results are essentially indistinguishable, suggesting that for practical purposes, they are simply different mathematical expressions for the same physics. The timescale in both simple models depends strongly on the time derivative of SST in the eastern Pacific in addition to the adjustment process affecting western Pacific SST. Thus, they both express essentially the same physics. The recharge oscillator, having a slightly more ad hoc derivation for western Pacific thermocline variations, is slightly easier to fit.
3) The JIN97 recharge oscillator and the SSBH delayed oscillator are both qualitatively plausible starting points for understanding ENSO oscillations. In the context of realistic ENSO variability as provided by a CGCM, however, the model's framework can be made substantially more complete by including an additional adjustment time between the wind stress and the eastern Pacific SST.
4) This additional adjustment time represents the coupled spinup of the atmosphere and the ocean mixed layer processes outside the equatorial eastern Pacific region on which the JIN97 and SSBH models focus. The strong effects of these additional coupled pro-

cesses on the ENSO cycle is consistent with mixed mode behavior.

Acknowledgments. We are grateful to F.-F. Jin and to anonymous reviewers for their comments on the original version of this manuscript. This study was supported by NOAA GOALS Grant NA66GP0370 and by NSF Grant Aim-0082529, and the NOAA CLIVAR-Pacific Program under Grants NA16GP1016 and NA16GP2003. Model integrations were performed at the San Diego Supercomputer Center (SDSC) and the Climate Simulation Laboratory (CSL) at NCAR.

REFERENCES

An, S.-I., and I.-S. Kang, 2000: A further investigation of the recharge oscillator paradigm for ENSO using a simple coupled model with the zonal mean and eddy separated. *J. Climate,* **13,** 1987–1993.

Battisti, D. S., 1988: The dynamics and thermodynamics of a warming event in a coupled tropical atmosphere/ocean model. *J. Atmos. Sci.,* **45,** 2889–2919.

——, and A. C. Hirst, 1989: Interannual variability in the tropical atmosphere/ocean system: Influence of the basic state, ocean geometry and nonlinearity. *J. Atmos. Sci.,* **46,** 1687–1712.

Bjerknes, J., 1966: A possible response of the atmospheric Hadley circulation to equatorial anomalies of ocean temperature. *Tellus,* **18,** 820–829.

——, 1969: Atmospheric teleconnections from the equatorial Pacific. *Mon. Wea. Rev.,* **97,** 163–172.

Blanke, B., J. D. Neelin, and D. Gutzler, 1997: Estimating the effects of stochastic wind stress forcing on ENSO irregularity. *J. Climate,* **10,** 1473–1486.

Bryan, K., 1969: A numerical method for the study of the circulation of the World Ocean. *J. Comput. Phys.,* **4,** 347–376.

Burgers, G., 1999: The El Niño stochastic oscillator. *Climate Dyn.,* **15,** 521–531.

Cane, M. A., and S. E. Zebiak, 1985: A theory for El Niño and the Southern Oscillation. *Science,* **228,** 1085–1087.

——, ——, and S. C. Dolan, 1986: Experimental forecasts of El Niño. *Nature,* **321,** 827–832.

Cox, M. D., 1984: A primitive equation three-dimensional model of the ocean. Tech. Rep. 1, GFDL Ocean Group, 75 pp.

Delecluse, P., M. Davey, Y. Kitamura, S. G. H. Philander, M. J. Suarez, and L. Bengtsson, 1998: Coupled general circulation modeling of the tropical Pacific. *J. Geophys. Res.,* **103,** 14 357–14 373.

Dijkstra, H. A., and J. D. Neelin, 1995: On the attractors of an intermediate coupled equatorial ocean–atmosphere model. *Dyn. Atmos. Oceans,* **22,** 19–48.

Eckert, C., and M. Latif, 1997: Predictability of a stochastically forced hybrid coupled model of El Niño. *J. Climate,* **10,** 1488–1504.

Jiang, N., J. D. Neelin, and M. Ghil, 1995: Quasi-quadrennial and quasi-biennial variability in COADS equatorial Pacific sea surface temperature and winds. *Climate Dyn.,* **12,** 101–112.

Jin, F.-F., 1997a: An equatorial recharge paradigm for ENSO. Part I: Conceptual model. *J. Atmos. Sci.,* **54,** 811–829.

——, 1997b: An equatorial recharge paradigm for ENSO. Part II: A stripped-down coupled model. *J. Atmos. Sci.,* **54,** 830–847.

——, and J. D. Neelin, 1993: Modes of interannual tropical ocean–atmosphere interaction—A unified view. Part I: Numerical results. *J. Atmos. Sci.,* **50,** 3477–3503.

——, ——, and M. Ghil, 1996: El Niño/Southern Oscillation and the annual cycle: Subharmonic frequency locking and aperiodicity. *Physica D,* **98,** 442–465.

Kleeman, R., and A. M. Moore, 1997: A theory for the limitation of ENSO predictability due to stochastic atmospheric transients. *J. Atmos. Sci.,* **54,** 753–767.

Latif, M., and Coauthors, 2001: ENSIP: The El Niño Simulation Intercomparison Project. *Climate Dyn.,* **18,** 255–276.

Mechoso, C. R., J.-Y. Yu, and A. Arakawa, 2000: A coupled GCM pilgrimage: From climate catastrophe to ENSO simulations. *General Circulation Model Development: Past, Present, and Future,* D. A. Randall, Ed., Academic Press, 539–575.

Neelin, J. D., 1991: The slow sea surface temperature mode and the fast-wave limit: Analytic theory for tropical interannual oscillations and experiments in a hybrid coupled model. *J. Atmos. Sci.,* **48,** 584–606.

——, and F.-F. Jin, 1993: Modes of interannual tropical ocean–atmosphere interaction—A unified view. Part II: Analytical results in the weak-coupling limit. *J. Atmos. Sci.,* **50,** 3504–3522.

——, M. Latif, and F.-F. Jin, 1994: Dynamics of coupled ocean–atmosphere models: The tropical problem. *Annu. Rev. Fluid Mech.,* **26,** 617–659.

——, D. S. Battisti, A. C. Hirst, F.-F. Jin, Y. Wakata, T. Yamagata, and S. E. Zebiak, 1998: ENSO theory. *J. Geophys. Res.,* **103,** 14 261–14 290.

——, F.-F. Jin, and H.-H. Syu, 2000: Variations in ENSO phase-locking. *J. Climate,* **13,** 2570–2590.

Pacanowski, R. C., K. W. Dixon, and A. Rosati, 1991: The GFDL Modular Ocean Model user guide. Tech. Rep. 2, GFDL Ocean Group, 232 pp.

Penland, C., and T. Magorian, 1993: Prediction of Niño-3 sea surface temperatures using linear inverse modeling. *J. Climate,* **6,** 1067–1076.

Rasmusson, E. M., X. Wang, and C. F. Ropelewski, 1990: The biennial component of ENSO variability. *J. Mar. Syst.,* **1,** 71–96.

Schopf, P. S., and M. J. Suarez, 1988: Vacillations in a coupled ocean–atmosphere model. *J. Atmos. Sci.,* **45,** 549–566.

Suarez, M. J., and P. S. Schopf, 1988: A delayed action oscillator for ENSO. *J. Atmos. Sci.,* **45,** 3283–3287.

Syu, H.-H., and J. D. Neelin, 2000: ENSO in a hybrid coupled model. Part I: Sensitivity to physical parameterizations. *Climate Dyn.,* **16,** 19–34.

Thompson, C. J., and D. S. Battisti, 2000: A linear stochastic dynamical model of ENSO. Part I: Model development. *J. Climate,* **13,** 2818–2932.

Torrence, C., and G. P. Compo, 1998: A practical guide to wavelet analysis. *Bull. Amer. Meteor. Soc.,* **79,** 61–78.

Wang, B., R. Wu, and R. Lukas, 1999: Roles of the western North Pacific wind variation in thermocline adjustment and ENSO phase transition. *J. Meteor. Soc. Japan,* **77,** 1–16.

Weisberg, R. H., C. Wang, and J. I. Virmani, 1999: Western Pacific interannual variability associated with the El Niño–Southern Oscillation. *J. Geophys. Res.,* **104,** 5131–5149.

Wyrtki, K., 1975: El Niño—The dynamic response of the equatorial Pacific Ocean to atmospheric forcing. *J. Phys. Oceanogr.,* **5,** 572–584.

Yu, J.-Y., and C. R. Mechoso, 2001: A coupled atmosphere–ocean GCM study of the ENSO cycle. *J. Climate,* **14,** 2329–2350.

Zebiak, S. E., 1989: Ocean heat content variability and El Niño cycles. *J. Phys. Oceanogr.,* **19,** 475–486.